AD-A094 324 SOUTHWEST RESEARCH INST SAN ANTONIO TEX F/G 11/2
COMPRESSIVE STRENGTH AND DAMAGE MECHANISMS IN CERAMIC MATERIALS--ETC(U)
SEP 80 J LANKFORD N00014-75-C-0668
UNCLASSIFIED NL

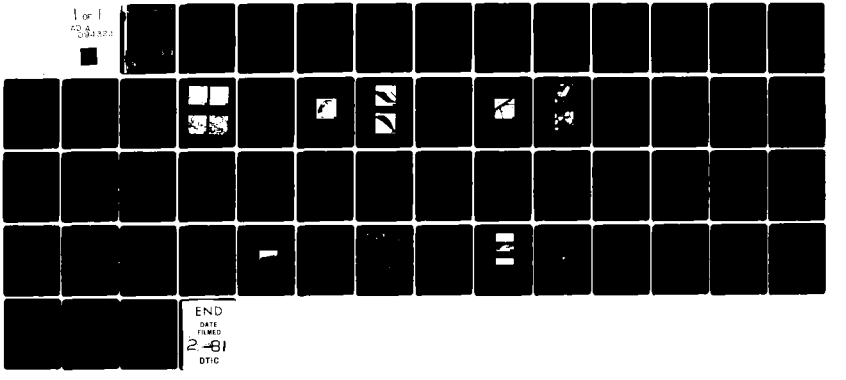

LEVEL III AD A071842 (2)

COMPRESSIVE STRENGTH AND DAMAGE MECHANISMS IN CERAMIC MATERIALS

I. Temperature-Strain Rate Dependence of Compressive Strength and Damage Mechanisms in Aluminum Oxide
II. Threshold Microfracture During Elastic-Plastic Indentation of Ceramics

by

James Lankford

INTERIM TECHNICAL REPORT

ONR Contract no. N00014-75-C-0668
ONR Contract Authority NR 032-553/1-3-75(471)
SwRI Project No. 02-4231

For

Office of Naval Research
Arlington, Va 22217

By

Southwest Research Institute
San Antonio, Texas

September 1980

SOUTHWEST RESEARCH INSTITUTE
SAN ANTONIO HOUSTON

UNCLASSIFIED

SECURITY CLASSIFICATION OF THIS PAGE (When Data Entered)

REPORT DOCUMENTATION PAGE

READ INSTRUCTIONS BEFORE COMPLETING FORM

1. REPORT NUMBER

2. GOVT ACCESSION NO. AD-A094 324

3. RECIPIENT'S CATALOG NUMBER

4. TITLE (and Subtitle)

Compressive Strength and Damage Mechanisms in Ceramic Materials.

5. TYPE OF REPORT & PERIOD COVERED
Interim Technical Report
1 Feb 1980 — 31 Aug 1980

6. PERFORMING ORG. REPORT NUMBER
02-4231

7. AUTHOR(s)

James Lankford

8. CONTRACT OR GRANT NUMBER(s)
N00014-75-C-0668

9. PERFORMING ORGANIZATION NAME AND ADDRESS
Southwest Research Institute
6220 Culebra Road (P. O. Drawer 28510)
San Antonio, TX 78284

10. PROGRAM ELEMENT, PROJECT, TASK AREA & WORK UNIT NUMBERS
NR 032-553/1-3-75(471)

11. CONTROLLING OFFICE NAME AND ADDRESS
Office of Naval Research
800 North Quincy
Arlington, VA 22217

12. REPORT DATE
10 September 1980

13. NUMBER OF PAGES
50 + prelims.

14. MONITORING AGENCY NAME & ADDRESS(if different from Controlling Office)

15. SECURITY CLASS. (of this report)
Unclassified

15a. DECLASSIFICATION/DOWNGRADING SCHEDULE

I. Temperature-Strain Rate Dependence of Compressive Strength and Damage Mechanisms in Aluminum Oxide. II. Threshold Microfracture During Elastic-Plastic Indentation of Ceramics.

16. DISTRI

APPROVED FOR PUBLIC RELEASE:
DISTRIBUTION UNLIMITED

17. DISTRIBUTION STATEMENT (of the abstract entered in Block 20, if different from Report)

18. SUPPLEMENTARY NOTES

19. KEY WORDS (Continue on reverse side if necessary and identify by block number)

Compressive Strength	Microcrack Initiation	Cracking Threshold
Temperature Effects	Ceramics	Fractography
Loading Rate	Aluminum Oxide	Fracture Mechanisms

20. ABSTRACT (Continue on reverse side if necessary and identify by block number)

The results of compression tests of Al_2O_3 performed over a wide range in temperature and strain rate are interpreted in terms of dominant damage mechanisms. It is shown that compressive failure in Al_2O_3 is caused by one of three different mechanisms, each based on tensile (Mode I) growth of predominantly axial microcracks, and each characteristic of a specific temperature-strain rate regime. The concepts developed should be applicable to other strong ceramics. In addition, indentation experiments were carried

DD FORM 1 JAN 73 1473 EDITION OF 1 NOV 65 IS OBSOLETE

UNCLASSIFIED

SECURITY CLASSIFICATION OF THIS PAGE (When Data Entered)

out for a variety of ceramics. It is found that the threshold for microfracture during elastic-plastic indentation corresponds to radial, rather than subsurface median, crack formation. This is contrary to the fundamental assumption of existing models for threshold crack nucleation by sharp indenters or particles; the results indicate the need to modify the stress field calculations used in these models.

FOREWORD

This report is based upon experiments carried out and reported earlier, as well as critical tests completed only in the last six months. Complete analysis of the temperature-strain rate dependence of Al_2O_3 compressive strength, as outlined herein, has required the interpretation of these several years of experimental research. The indentation work described here also involves both recent and earlier, but not previously analyzed, experiments.

TABLE OF CONTENTS

LIST OF FIGURES

LIST OF FIGURES (CONTINUED)

I

THE TEMPERATURE-STRAIN RATE DEPENDENCE OF COMPRESSIVE STRENGTH AND DAMAGE MECHANISMS IN ALUMINUM OXIDE

James Lankford

Department of Materials Sciences
Southwest Research Institute
San Antonio, Texas 78284, USA

ABSTRACT

The results of compression tests of Al_2O_3 performed over a wide range in temperature and strain rate are interpreted in terms of dominant damage mechanisms. It is shown that compressive failure in Al_2O_3 is caused by one of three different mechanisms, each based on tensile (Mode I) growth of predominantly axial microcracks, and each characteristic of a specific temperature-strain rate regime. The concepts developed should be applicable to other strong ceramics.

1. Introduction

Damage caused by compressive loading is an important consideration in a number of technological applications of high strength ceramics. Such situations arise, for example, during operation of turbines, in which thermal cycle-induced compressive stresses may be produced; in other cases, turbines may be preloaded in compression, to minimize tensile loads. In addition, compressive microfracture probably is an important failure mode during particle

impact (erosion) of ceramic radomes, IR windows, and turbine blades, and during wear of ceramic bearing surfaces.

Like tensile fracture, failure under compressive loading has been recognized as a process which is dependent upon both temperature and loading rate. However, it has generally been assumed that tensile and compressive fracture are fundamentally different. The present objective is to bring together the results of an experimental investigation of aluminum oxide which has extended over several years [1,2], including recent tests carried out at high temperatures and strain rates, and to interpret these results in terms of current failure models. It will be suggested that for strong ceramics like Al_2O_3, both tensile and compressive failure actually occur through basically identical microfracture processes; the principal difference being that compressive failure involves multiple cracks, while tensile fracture occurs through the action of a single dominant crack.

2. Experimental Procedure

Specimen preparation and testing procedures have previously been described [1-3]. Briefly, 0.625 in. dia. x 1.25 cm long right circular cylinders of Lucalox polycrystalline α-alumina* were

---

*General Electric Lamp Glass Division, Cleveland, Ohio, USA.

loaded to failure in compression. Experiments were performed at strain rates of $7\times10^{-5}s^{-1}$ and $2\times10^{-1}s^{-1}$ using a standard servo-controlled hydraulic test machine, and at $\sim2\times10^{3}s^{-1}$ in a Hopkinson pressure bar. Temperature was varied from 77° to 1800°K; over this range the development of compressive damage was monitored for the lowest strain rate using acoustic emission. Failed specimens were studied fractographically in the scanning electron microscope (SEM). The latter also was used to characterize microscopic compressive damage manifested on the outer surfaces of highly stressed specimens subjected to various temperature-strain rate combinations.

3. Results

3.1 Compression Tests

Compressive strength (σ_c) as a function of temperature (T) for all three strain rates ($\dot{\varepsilon}$) is shown in Fig. 1, together with the stress level corresponding to the onset of acoustic emission (σ_{AE}). Also shown is a data point representing recent Hugoniot shock measurements ($\dot{\varepsilon} \gtrsim 10^{4}s^{-1}$) carried out by Munson and Lawrence [4] on Lucalox. Of particular interest are the strength increase between 500 and 700°K, the decrease in σ_c and σ_{AE} for $T > 900°K$, and the total suppression of acoustic emission for $T \gtrsim 1300°K$. Linear extrapolation of the low temperature (region I) σ_c data shows that they converge at $T = 0°K$ to a strength of

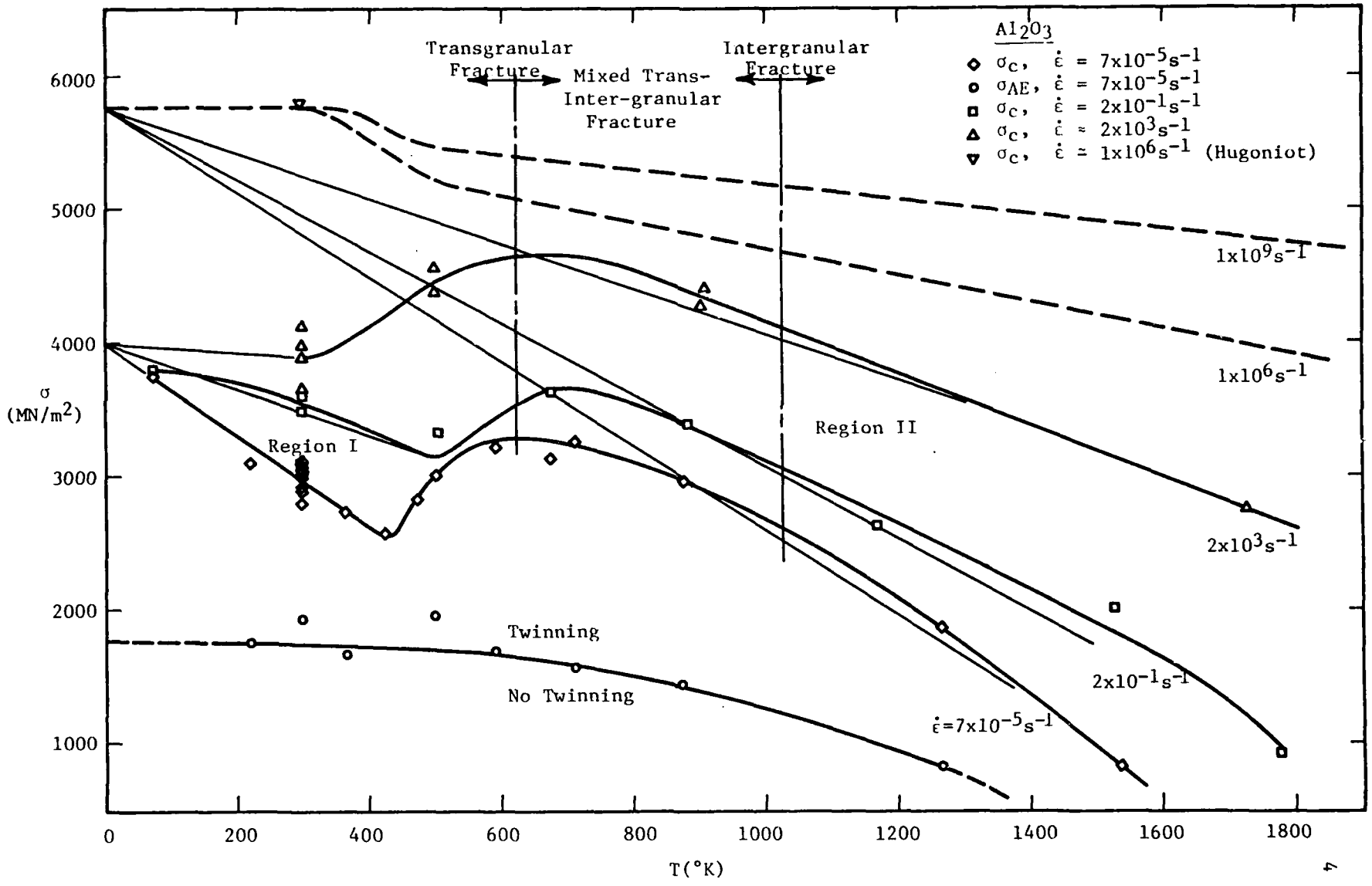

Figure 1. Compressive Strength Versus Temperature as a Function of Strain Rate.

approximately 4075 MN/m^2. Similarly, the high temperature (region II) results extrapolate to a stress level of 5750 MN/m^2 at absolute zero. Regions I and II are connected by a transition region, corresponding to a change in fracture mode (discussed shortly).

The low temperature stress level for twinning was determined by SEM observation. Earlier work [2], reporting an upward trend in σ_{AE} with decreasing T, erred in that the background AE level was too high, due to liquid nitrogen "noise" (bubbles), thereby masking the true twinning stress threshold. Microscopic inspection indicates that the twinning threshold actually is essentially athermal.

Additional aspects of the experimental results are apparent upon replotting them in the form σ_c versus log $\dot{\varepsilon}$, as shown in Fig. 2. Here the regions I and II data again converge, at $\dot{\varepsilon} \cong 10^5$ and $5 \times 10^{12} s^{-1}$, respectively. However, in the case of the room temperature region I plot, there is an abrupt acceleration in the rate of increase in strength with strain rate (region III), beginning at $\dot{\varepsilon} \gtrsim 10^3 s^{-1}$; at this point, the slope of $\sigma_c(\dot{\varepsilon})$ increases by more than an order of magnitude, from ~.02 to ~.27. Finally, by inspection, it is possible to deduce effective strength levels which would obtain at strain rate levels too high to achieve in normal controlled tests. This process yields the predicted $\sigma_c(T)$ plots shown in Fig. 1 for $\dot{\varepsilon} = 10^6$ and $10^9 s^{-1}$.

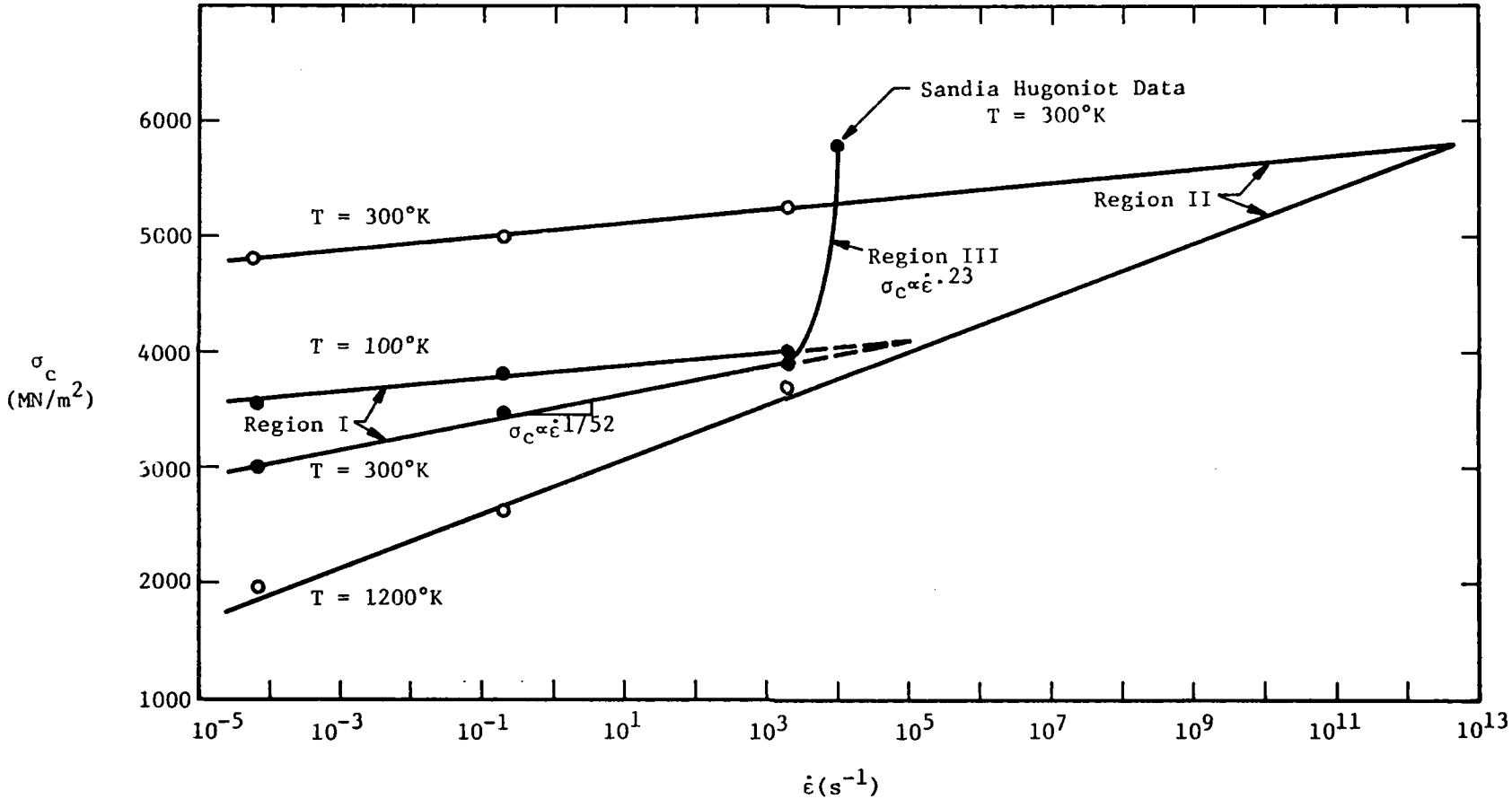

Figure 2. Compressive Strength Versus Strain Rate as a Function of Temperature, Showing Three Damage Regimes.

Acoustic emission was obtained in terms of total counts (N) in excess of a minimum threshold level versus both increasing compressive stress σ and time t. N(t) was differentiated to yield $\frac{dN}{dt}(\sigma)$, as shown in Fig. 3. Also shown is the result of acoustic emission during bending of a ground, hence pre-microcracked, specimen of Lucalox [5]. The first stage (slope S_1=5) of the compressive $\frac{dN}{dt}(\sigma)$ relationship has been identified [3] with crack nucleation, while the acoustic emission response of the tensile specimen has no such first stage, and has been shown to represent tensile microcrack extension prior to fracture [5].

3.2 Fractographic Analysis

The fractographic features associated with failure over a wide temperature range are shown in Fig. 4. At 77°K [Fig. 4(a)] the failure surface is principally transgranular, with only occasional intergranular features, while at 743°K [Fig. 4(b)], somewhat more intergranular fracture is present. In both photos, the transgranular regions appear rather smooth, but noncrystallographic. This situation changes as higher temperatures are attained; at 1190°K, for example, the fracture is predominantly intergranular and the relatively few transgranular regions (arrows) differ in appearance from those characteristic of lower temperatures; rather than being flat, they are composed mostly of jagged, straight-edged crystallographic steps [Fig. 4(c)]. At still higher temperatures, fracture is almost entirely intergranular (Fig. 4(d), T = 1560°K). In fact,

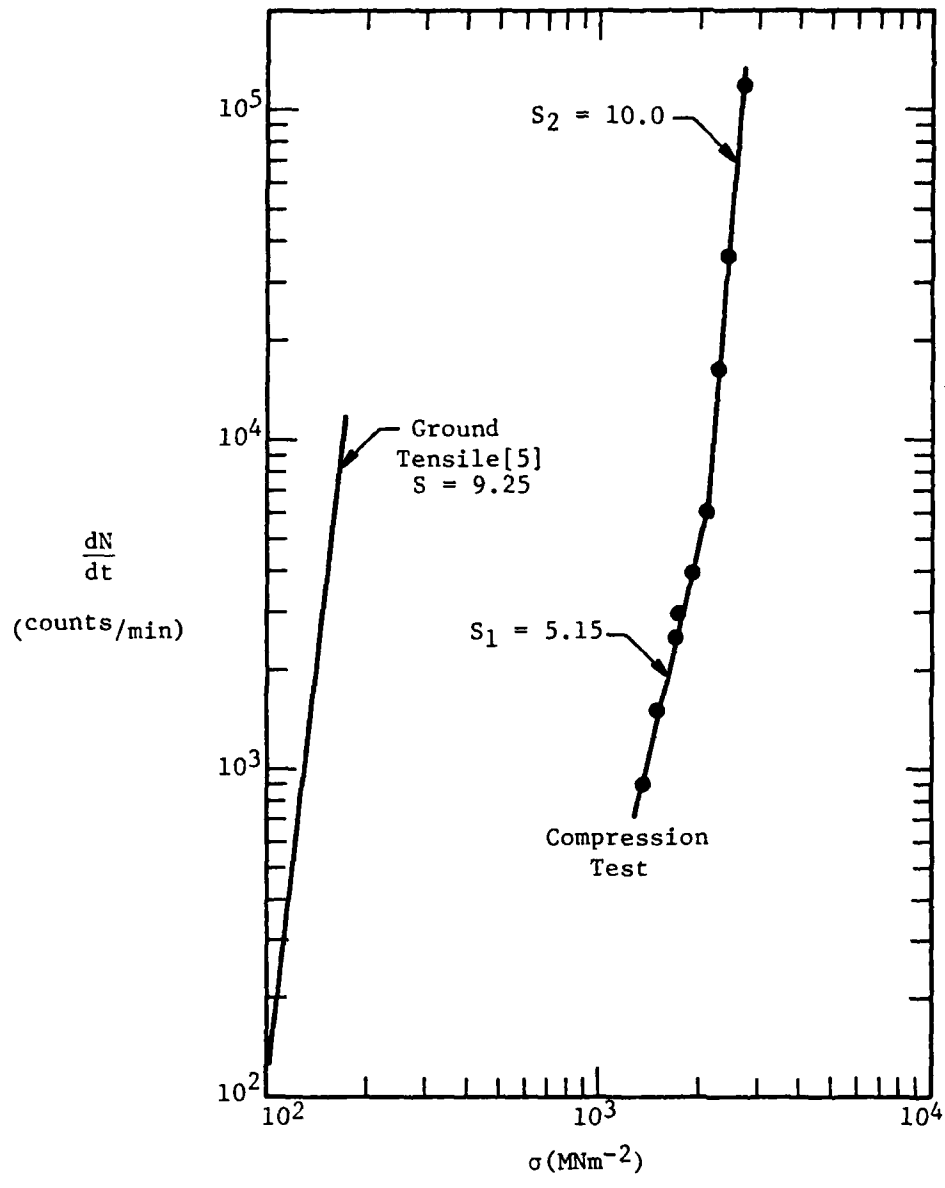

Figure 3. Acoustic Emission Count Rate Versus Applied Stress for Lucalox, T = 300°K.

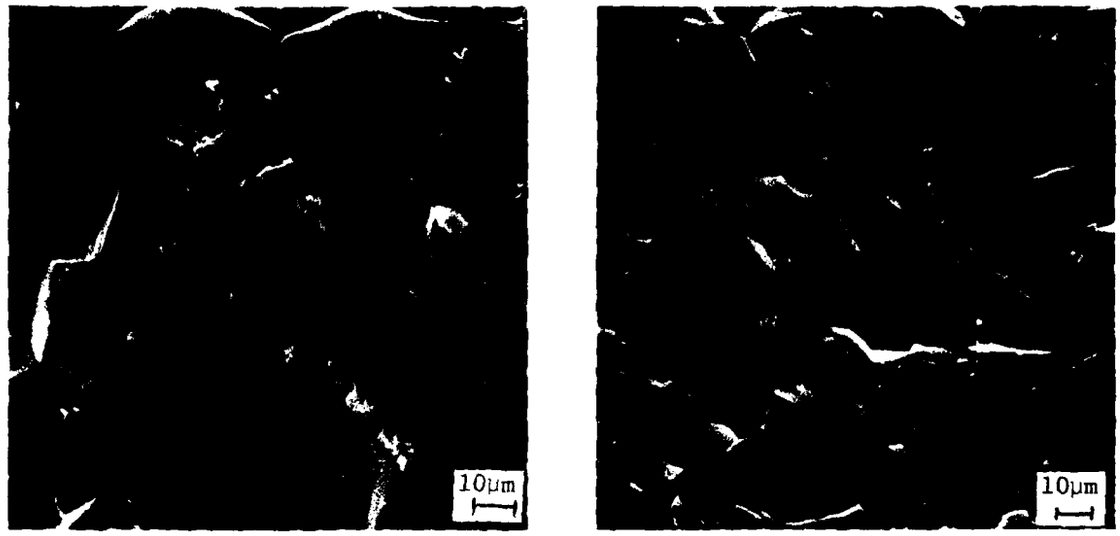

(a) T = 77°K

(b) T = 743°K

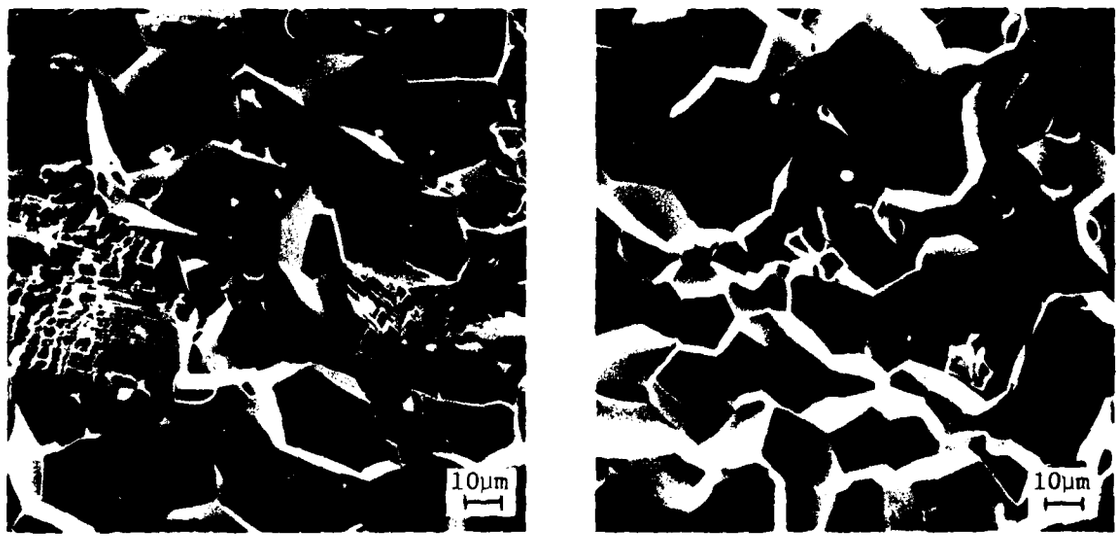

(c) T = 1190°K

(d) T = 1560°K

Figure 4. Fracture Surfaces for Al_2O_3 Failed Under Compression, $\dot{\epsilon} = 7 \times 10^{-5}$ sec^{-1}.

fracture is so intergranular that the "dust" to which most of the test specimen is reduced consists of individual, perfect crystallites of sapphire. This is true even for strain rates on the order of $10^3 s^{-1}$, as shown in Fig. 5.

It should be noted that bending (tensile) tests on Lucalox have been carried out [6] at an intermediate loading rate over (essentially) the same temperature range. The fractographic observations made on these specimens were basically identical to those described above for compressive failure.

Further fractographic detail is visible at higher magnification. In Fig. 6, it can be seen that at 900°K, the intergranular facets are almost perfectly smooth and featureless. For $T \gtrsim 1300°K$, on the other hand, careful study shows that for all loading rates, the facets are covered with a multitude of what appear to be the remains of a liquid phase which has agglomerated into solidified globules [Fig. 6(a)]. It should be emphasized that these globules are not fracture debris; each compressive fracture fragment was immersed in alcohol and cleaned ultrasonically prior to coating for SEM study. For tests carried out at $T < 1300°K$, this process produces facets which are perfectly devoid of such globules [Fig. 6(b)].

3.3 Microplasticity Observations

From 77° to ~900°K, the only evidence of microplasticity is the formation of twins, as discussed elsewhere [1]. The

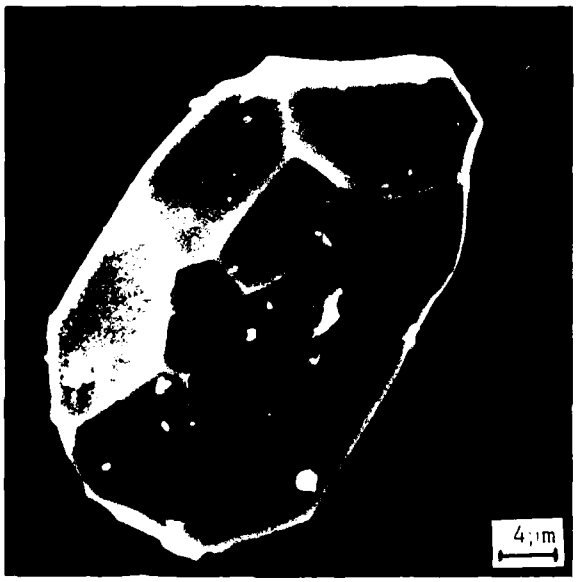

Figure 5. Particulate (Crystallite) Remnant of Al_2O_3 Compressive Failure, $\dot{\varepsilon} = 2 \times 10^3 s^{-1}$, T = 1800°K.

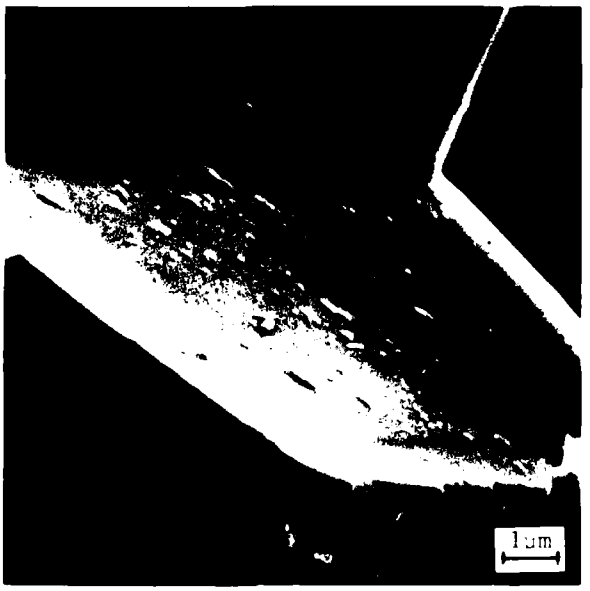

a) Globular Glassy Phase, $\dot{\varepsilon} = 2 \times 10^{3} s^{-1}$, T = 1800°K

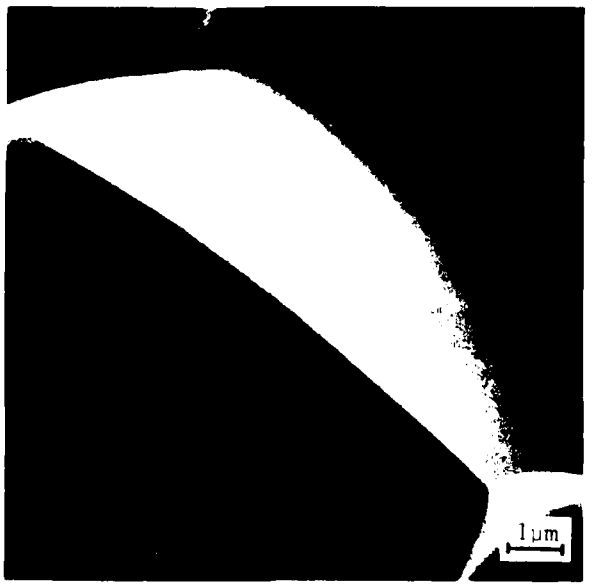

b) Smooth Facet, $\dot{\varepsilon} = 7 \times 10^{-5} s^{-1}$, T = 900°K

Figure 6. Al_2O_3 Intergranular Facets Attending Compressive Failure.

significance of these twins is that they nucleate microcracks, as shown in Fig. 7, particularly within grains adjacent to grain boundaries impinged upon by twins. Above 900°K, twins still form, but they are now much thicker [Fig. 8(a)], and have less propensity to form cracks. Twinning cracks which do form are located at the twin-parent interface, rather than being the product of the twin impacting a grain boundary, as is common at lower temperatures. In fact, once the few twin-nucleated microcracks encounter grain boundaries, they change mode to intergranular [Fig. 8(b)]. Generally, higher temperature microcracks form along grain boundaries, often nucleating at the triple points, and remain intergranular as the crack grows [Fig. 8(a)]. Although some evidence of possible dislocation activity was seen, it was not extensive.

It should be noted that the process of microcracking itself represents a form of plasticity. The predominant microcrack orientation observed, regardless of temperature or strain rate, was (near) axial, i.e., the compression axis tended to lie in the plane of the crack.

4. Analysis of Damage Mechanisms

In the following sections, the compressive failure of Al_2O_3 will be analyzed based on the foregoing experimental observations. To simplify the discussion, three regions of failure will be

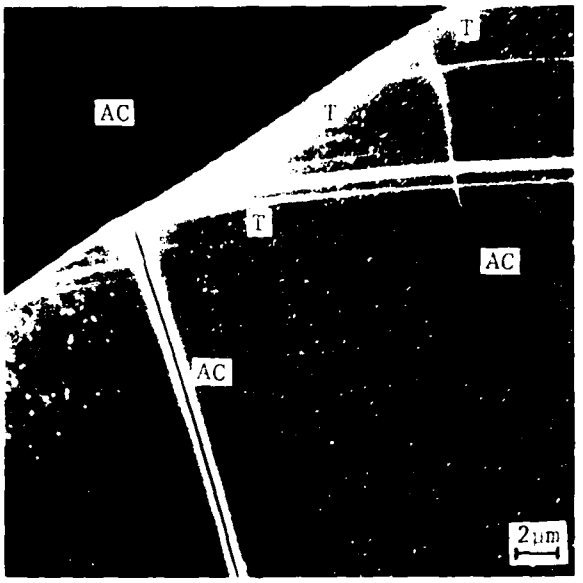

Figure 7. Crack Initiation in Al_2O_3 Under Compressive Loading, $T \geq 900°K$, Compression Axis Vertical, Axial Cracks (AC), Twins (T).

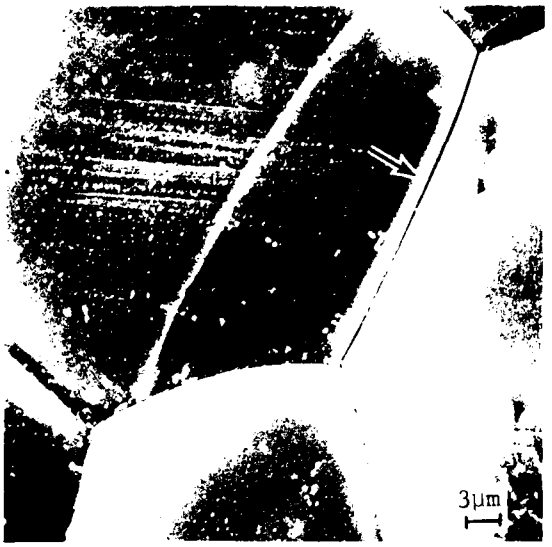

(a) Twinning (T) with no cracking; axial intergranular cracking (arrow); T = 1560°K

(b) Transition from twin (T) - nucleated, transgranular (~ axial) cracking to intergranular (~ axial) cracking (arrow); T = 1560°K

Figure 8. Crack Initiation in Al_2O_3 Under Compressive Loading, T ~ 900°K, Compression Axis Vertical.

considered, as exemplified in Fig. 2: (1) a thermally-activated, low temperature regime, in which $\dot{\varepsilon} \lesssim 10^3 s^{-1}$; (2) a thermally-activated, high temperature regime; (3) a low temperature regime characterized by $\dot{\varepsilon} > 10^3 s^{-1}$ (this regime may extend to high temperature as well).

4.1 Region 1: $0 \lesssim T \lesssim 500°K$, $\dot{\varepsilon} \lesssim 10^3 s^{-1}$

In this regime, three basic processes appear to cause a specimen to fail, namely, (1) twins nucleate, forming associated axial microcracks, which (2) grow, and eventually (3) coalesce at failure. At least one of these processes must be thermally activated, to account for the observed strain rate-temperature dependence of σ_c.

It is not expected that crack coalescence can account for this effect, since coalescence occurs only in the last instant of compressive failure. Similarly, from the apparent temperature insensitivity (Fig. 1) of the twinning threshold, crack nucleation* does not seem to exhibit the requisite thermally activated character.

---

*It was shown in detail in earlier work that twinning is the sole source of microfracture in this regime. Thus, the question of thermally activated microcrack nucleation is directly tied to that of concurrent twinning.

Since two of the possibilities can be minimized, it therefore seems necessary to consider first whether axial cracks in uniaxial compressive stress fields could experience local tensile loading, and if so, whether thermally-activated growth of such cracks might explain the observed strength behavior. In Fig. 9, a twin nucleated in grain 1 by the applied compressive stress σ impinges upon the grain boundary, forming an axial microcrack (recall Fig. 7). If the grains are misoriented, so that their effective moduli (E') mismatch across the boundary in such a way that the upper grain is compliant relative to the stiffer lower grain, then a local tensile stress will exist at the interface [7]. This stress will be proportional to the difference in ν/E', where ν is Poisson's ratio. Radial tension therefore will occur on the stiff side, reaching significant fractions of the applied compressive stress for only small differences in ν/E' between the two grains [8]. Other microscopic scenarios as well have been suggested and observed which indicate the presence of tensile stresses across axial cracks in compressive specimens [9-11].

Under flexural (tensile) loading, the tensile strength σ_t of alumina, as for most ceramics, obeys a law of the form [12]

$$\sigma_t = B\,\dot{\varepsilon}^{1/(1+n)} \tag{1}$$

It turns out that n also is equal to the region I power-law exponent in the empirical stress intensity (K_I) - Mode I crack velocity (V) relationship [12]

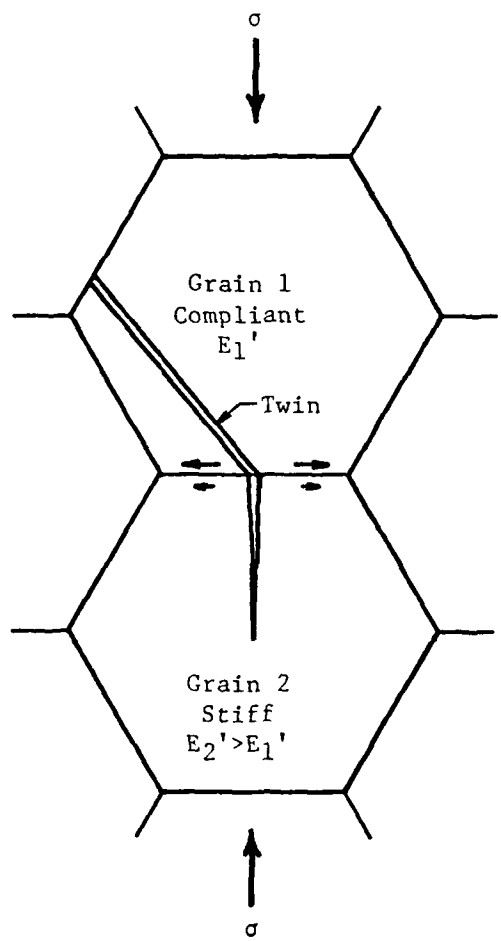

Figure 9. Conceptual Sketch of Resolution of Applied Compressive Stress into Local Tensile Stress Normal to Plane of Axial Microcrack. Interfacial arrows represent unequal elastic lateral displacements in the two grains, producing local tensile stress field at the interface [7].

$$V = AK_I^n \tag{2}$$

For Lucalox, room temperature experiments of the latter sort show that n = 52 [5]. In the present compression experiments, it is possible to represent σ_c versus $\dot{\varepsilon}$ at room temperature (Fig. 2) by

$$\sigma_c = c\,\dot{\varepsilon}^{1/(1+n')} \tag{3}$$

in which case n' = 51. The excellent agreement between n' and n suggests, by analogy with the correlation of Equations (1) and (2) through n, that the strain rate dependence of σ_c is controlled by thermally activated subcritical growth of Mode I axial cracks.

Further support for this proposition derives from consideration of the acoustic emission data. As shown in Fig. 3, the slope S_2 = 10 of the second stage of the $\frac{dN}{dt}$ versus compressive stress relationship is identical to the slope of the corresponding curve for the ground, pre-microcracked tensile specimen, in which the AE is known [5] to be caused by microcrack growth. Thus, Mode I microcrack extension again is implicated.

Finally, the apparent activation energy for the thermally activated process in question can be calculated using the data of Figs. 1 and 2. For ceramic materials, one may usually write [13]

$$\dot{\varepsilon} = \dot{\varepsilon}_o \exp\left[\frac{-H(\sigma_c)}{RT}\right] \tag{4}$$

where $\dot{\varepsilon}_o$ is a frequency factor, and $H(\sigma)$ an activation energy. If we assume a linear relationship between H and σ_c, we see that

$$H = H_o - V(\sigma_c - \sigma_o) \tag{5}$$

where V is an activation volume, and σ_o a threshold stress level. In this case, we will ignore σ_o, as it does not affect the ensuing calculation to a significant extent. Thus

$$H = H_o - V\sigma_c \tag{6}$$

At $T = 0$, $\sigma = \sigma_c^{(o)}$, hence

$$\sigma_c^{(o)} = \frac{H_o}{V} \tag{7}$$

Similarly, at $T = T_1$, $\sigma_c = \sigma_c^{(1)}$, or

$$\sigma_c^{(1)} = \frac{H_o}{V} - \frac{RT_1}{V} \ln\left(\frac{\dot{\varepsilon}_o}{\dot{\varepsilon}_1}\right) \tag{8}$$

Combining Equations 7 and 8 to eliminate V yields

$$H_o = \frac{RT_1 \, \sigma_c^{(o)}}{\sigma_c^{(o)} - \sigma_c^{(1)}} \ln\left(\frac{\dot{\varepsilon}_o}{\dot{\varepsilon}_1}\right) \tag{9}$$

Using data shown in Fig. 2, we find that $H_o \simeq 45$ kcal/mole. This is a relatively low activation energy, of the same order as values obtained for (ambient) slow crack tests in soda lime glass

(26 kcal/mole) [14] and silicon carbide (~30 kcal/mole) [15]. Equivalent data for Al_2O_3 are unavailable.

4.2 Region 2: $T \gtrsim 700°K$, $\dot{\varepsilon} \lesssim 10^3 s^{-1}$

In this regime, fracture is no longer transgranular, and microcracks have much less tendency to form via twinning. For $T \gtrsim 1000°K$, fracture is almost entirely intergranular, and apparently related to flow (cavitation) in a thin grain boundary phase. The nature of the latter phase is unclear, despite a great deal of recent surface chemistry work [16-19] on Lucalox aimed at establishing its grain boundary chemistry. Based on Auger electron spectroscopy, the only elements present in significant concentrations at the boundaries seem to be aluminum, oxygen, and calcium, although Si, which is difficult to detect, may be present in small quantities [20]. The presence of Si in addition to the other elements detected could account for a low melting point ($T_{mp} \lesssim 1500°K$) glass phase. This point requires further study.

Clearly, however, a grain boundary phase is present, and it is possible to show that cavitation in it is compatible with the observed $\sigma_c(T, \dot{\varepsilon})$ dependence. In particular, Evans and Rana [21] have recently developed a statistical model of high temperature ceramic failure through viscous growth of cavities in a thin grain boundary phase. Although the model is derived in terms of constant stress creep experiments, i.e., creep lifetime, it can be used to estimate approximate time to failure for constant strain rate experiments as well.

For example, the most extreme test of the model would be to predict the results of the pressure bar experiments, where the strain rates are approximately nine orders of magnitude higher than conventional creep rates. Let us consider the results of pressure bar tests at 1800°K, for which the compressive failure strength is 2650 MN/m^2. The actual time to failure is given by

$$t_f = {}^{\sigma_c}/E\dot{\varepsilon} \tag{10}$$

where E is the modulus of elasticity. In this case, E is reduced by the elevated temperature [22] to ~194 GN/m^2, and with $\dot{\varepsilon} \sim 10^3 s^{-1}$, $t_f \approx 14 \mu sec$.

According to Evans and Rana, in a material containing a continuous second phase, cavitation should occur primarily within the second phase by viscous deformation. For high strength ceramics at reasonably high applied stress levels, the time t_p for the formation of facet-sized cavities can be approximated by [21]

$$t_p \approx 0.15({}^{\eta_o}/\sigma_\infty)({}^{\ell}/\delta_o)^2 \exp({}^{Q_\eta}/RT) \tag{11}$$

where η_o is a constant, σ_∞ is the applied stress, ℓ is the mean dimension of a facet, $2\delta_o$ is the initial thickness of the viscous phase, and Q_η is the activation energy for viscous flow. If we assume that the compressive failure event corresponds to the (essentially) instantaneous coalescence of such microcrack cavities, then we can roughly equate t_p with t_f. It is further assumed that

the cavities form on axially oriented grain boundary facets, due to resolved tensile stresses.

To determine whether this is reasonable, it is necessary to evaluate Equation 11 using the appropriate parameters. The average compressive stress during the course of the constant strain rate test is $\sigma_c/2$; if the average tensile stress resolved across an axially-oriented facet is assumed to be approximately half of the latter, then $\sigma_\infty \approx 660$ MN/m^2. The average facet dimension is ~25μm, and a reasonable estimate for the film thickness δ_o is ~5 nm [21]. Based on tensile rupture experiments carried out by Walles [23] on Al_2O_3 fibers, Evans and Rana determined that $\eta_o(\ell/\delta_o)^2 \sim 10^6$ poise. Using the preceding values for ℓ and δ_o in this relationship yields $\eta_o \sim 10^{-2}$ poise. Finally, Q_η can be calculated from Fig. 2 using Equation 9 (setting $Q_\eta = H_o$), which provides an activation energy of 134 kcal/mole. This value shows reasonable agreement with that found by Walles [23], i.e., 115 kcal/mole. Incorporation of these numerical terms into Equation 11 yields a predicted failure time (for $\dot{\varepsilon} \sim 10^3 s^{-1}$, T = 1800°K) of ~29μsec. Considering the approximations involved, agreement with the actual failure time of ~14μsec is considered good.*

4.3 Region 3: $\dot{\varepsilon} \gtrsim 10^3 s^{-1}$

A sudden increase in the dependence of strength upon strain rate at high loading rates is an effect which has been noted recently for several types of rock [24], as well as for SiC [2].

*Comparison of t_p with t_f for the lower $\dot{\varepsilon}$ nearer classical creep rates showed similar relative agreement.

In the latter case, the enhanced strain rate dependence showed up in Hopkinson bar experiments, with the break occuring at $\dot{\varepsilon} \sim 10^2 s^{-1}$. Thus, the existence of region 3 shown in Fig. 2, i.e., the departure of the Sandia data from the present experimental results, is considered to represent a real physical phenomenon.

In a recent series of papers, Grady and his colleagues [24-26] have addressed this behavior as it pertains to rocks, developing a formalism for treating the rate dependence of fracture and fragmentation which is based upon inertial effects associated with the finite activation and growth times of the inherent flaw structure. One of the principal predictions of this analysis is that for situations in which dynamics (as opposed to subcritical, thermally activated mechanisms) are controlling fracture, strength should be proportional (approximately) to $\dot{\varepsilon}^{1/3}$ [24]. In the present case, Fig. 2 shows that in region 3, $\sigma_c \propto \dot{\varepsilon}^{.27}$, in reasonable agreement with the crack inertia concept, particularly considering that the model has been formulated for tensile loading.

It is possible to analyze this concept further. As pointed out by Grady and Kipp [25], crack activation in general, i.e., static or dynamic, can be considered to be governed by a Weibull distribution of the form

$$N = k \varepsilon^m \tag{12}$$

where N is the number of flaws which will activate at or below a tensile strain level ε, and k and m are distribution fracture

parameters. Further, it was shown that the static mean (tensile) fracture stress can be written as

$$\bar{\sigma}_M = I_m E(kV)^{-1/m} \tag{13}$$

where I_m is a constant, and V is the specimen volume.

It turns out that k and m are also critical parameters in relationships derived by Grady and Kipp [25] for dynamic fracture strength and fragment size L_M in the high loading rate, flaw inertia-controlled regime. By using these relationships in conjunction with measured dynamic σ_c and L_M values, k and m can be established, and used in Equation 13 to predict the static tensile fracture strength. Comparison of the latter with $\bar{\sigma}_M$ found experimentally then serves as an indirect test of the applicability of the crack inertia* concept.

At compressive fracture coalescence, fracture surfaces consisting of axially-oriented microcracks will form the sides of fragments having a mean size [25]

---

*Strictly speaking, one means material inertia, since a crack has no mass. However, this is not a material property effect, like the thermally-activated processes discussed earlier, but simply a consequence of a crack growing rapidly in any real, inertial material.

$$L_M = \frac{6C_g}{m+2} \alpha^{-\frac{1}{m+3}} \dot{\varepsilon}^{-\frac{m}{m+3}} \tag{14}$$

where C_g is the average velocity at which cracks activated under the applied load grow, and α is given by

$$\alpha = \frac{8\pi C_g^3 k}{(m+1)(m+2)(m+3)} \tag{15}$$

The dependence of fracture stress σ_M upon strain rate is given by

$$\sigma_M = E(m+3)(m+4)^{-\frac{(m+4)}{(m+3)}} \alpha^{-\frac{1}{m+3}} \dot{\varepsilon}^{\frac{3}{m+3}} \tag{16}$$

In the present case, we equate σ_M with the compressive failure stress σ_c, for which we have already observed $\sigma_c \alpha \dot{\varepsilon}^{.27}$. Thus, from Equation (16), $\frac{3}{m+3} = 0.27$, hence $m \approx 8$.

The parameter k is obtained by substituting Equation (15) into Equation (14) and solving for k, using appropriate values for the remaining terms. Fragments generated in the Hopkinson bar experiments, in which $\dot{\varepsilon} = 10^3 s^{-1}$, were examined in the SEM, and determined to have an average dimension of $L_M \approx 200\mu m$. With m=8, $\dot{\varepsilon} = 2 \times 10^3 s^{-1}$, and assuming that C_g is approximately 10% of the sound velocity in the material, i.e., $C_g \approx 1 \times 10^3 m/s$, k is found to be $3.5 \times 10^{36}/m^3$.

Using the preceding values for k and m, $\bar{\sigma}_M$ can be calculated. For m=8, I_m has been estimated as ≈ 1.0. Static tensile tests of Lucalox were previously [3] carried out in 3-point bending,

for which it is estimated that the stressed volume was approximately $6 \times 10^{-9} m^3$. Thus, Equation 13 yields a calculated $\bar{\sigma}_M$ of 120 MN/m^2, which, considering the approximations involved, compares reasonably well with the experimental value of 215 MN/m^2 [3].

5. Discussion

It is concluded that compressive failure in Al_2O_3 can be described in terms of three variants of axial cracks growing under the influence of local tensile stress fields. One process involves thermally activated growth of subcritical, transgranular cracks, nucleated athermally by twins formed over a characteristic stress range. At higher temperature, the efficiency of the twins as crack initiators drops, as their character is altered through a thickening process. Concurrently, the grain boundaries become sites of microcrack initiation through thermally activated viscous flow and cavitation. Since the nucleating twins lose some of their effectiveness at temperatures below which the grain boundaries are yet unable to flow easily, there is an apparent strengthening effect in this intermediate temperature range (600-900°K, Fig. 1).

Finally, for $T \lesssim 500°K$ (and possibly for much higher temperatures*) failure at impact-loading rates is controlled by a crack velocity (i.e., non-thermally activated), highly strain rate-sensitive process. The quantitative predictions of analytical models based upon each of these concepts are fulfilled by the results of the compressive experiments.

The results of this study have strongly implicated a critical role for tensile axial cracks in compressive failure. This concept is supported by a large recent body of work in the rock mechanics literature, in which dilatancy of compressive specimens has been explained in terms of the tensile opening of axial microcracks [28]. Recent observations by Kranz [9] have in fact confirmed the tensile character of compression-induced axial microcracks in granite. Finally, the writer has shown [29] that the strain rate dependence of compressive strength in limestone (which fails in a manner similar to granite) can be explained quantitatively by the same tensile microcrack growth concepts invoked in the present paper.

---

*There is no obvious reason why the crack inertia effect should not prevail at elevated temperatures as well. However, verification of this point will require high temperature failure tests at rates in excess of those generated in the Hopkinson pressure bar. If the mechanism is operative at elevated temperatures, the curve in Fig. 2 for $\dot{\varepsilon} = 10^6$ and $10^9 s^{-1}$ would move to higher stresses.

Aluminum oxide is usually considered to be a model brittle material; aside from its twinning propensity, its mechanical behavior is similar to that of other strong ceramics. There is thus good reason to believe that the several compressive failure regimes outlined here for Al_2O_3 should be observed in other engineering ceramics (and many rocks) as well. In the case of SiC and Si_3N_4, for instance, crack initiation should occur at the sharp-edged micropores characteristic of their microstructures, and such initiation probably would be athermal. Observation of compressive crack nucleation in SiC already suggests [30] that the pores do indeed nucleate axial cracks.

On the other hand, for materials like MgO, which can deform plastically at relatively low temperatures and thereby nucleate slipband cracks, there probably is a thermally activated crack nucleation mechanism superimposed upon that of subcritical crack growth. This would complicate the failure analysis, which was simplified in the present case by the absence of such considerations. Similarly, ceramics such as sintered α-SiC and NC-350 silicon nitride apparently have no viscous grain boundary film. In this case, high temperature failure would proceed by a mechanism such as grain boundary diffusion, for example, rather than viscous phase cavitation; this obviously would alter the failure criterion, and yield a different functional dependence for crack growth.

For a given brittle ceramic material, quantitative changes in its compressive strength can be accounted for through the thermally-activated and inertial models of tensile crack extension which have been discussed. However, the general strength level of the ceramic will depend upon its initial flaw distribution and character (pores, their relative smoothness, microcracks, minor second phases, etc.), and the ease with which flaws are produced (twinning, slip, phase transformation), since it is these crack nucleation factors which determine the stress level and initial size at which axial microcracks are able to begin to grow. This suggests that specific attention should be directed at understanding and characterizing these nucleation processes in various ceramics.

ACKNOWLEDGEMENTS

The writer is grateful to D. L. Davidson and U. S. Lindholm for their helpful comments, to H. Muehlenhaupt for his excellent experimental work in performing the compression experiments, and to M. Luckey for his careful specimen preparation. Support of the Office of Naval Research under Contract No. N00014-75-C-0668 is greatly appreciated.

REFERENCES

1. J. Lankford, J. Mater. Sci. 12 (1977) 2195.
2. J. Lankford and D. L. Davidson, Proc. Third Int. Conf. Mech. Behav. Mater., Vol. 3 (1979) 35.
3. J. Lankford, J. Mater. Sci. 13 (1978) 351.
4. D. E. Munson and R. J. Lawrence, J. App. Phys. 50 (1979) 6272.
5. A. G. Evans, M. Linzer, and L. R. Russell, J. Mater. Sci. 15 (1974) 253.
6. O. Johari and N. M. Parikh, Frac. Mech. Cer., Vol. 1, ed. R.C. Bradt, D.P.H. Hasselman, and F.F. Lange, Plenum Press, N.Y. (1974) 399.
7. P. Tapponier and W. F. Brace, Int. J. Rock Mech. Min. Sci. & Geomech. Abstr. 13 (1976) 103.
8. B. T. Brady, Int. J. Rock Mech. Min. Sci. 8 (1971) 357.
9. R. L. Kranz, Int. J. Rock Mech. Min. Sci. & Geomech. Abstr. 16 (1979) 23.
10. E. G. Bombolakis, Tektonophysics 1 (1964) 343.
11. S. Kobayashi, J. Soc. Mater. Sci. Jap. 20 (1971) 164.
12. A. G. Evans and S. M. Wiederhorn, Int. J. Frac. 10 (1974) 379.
13. K. C. Radford and G. R. Terwilliger, J. Am. Cer. Soc. 58 (1975) 274.
14. A. G. Evans, J. Mater. Sci. 7 (1972) 1137.
15. A. G. Evans and F. F. Lange, J. Mater. Sci. 10 (1975) 1659.

16. H. L. Marcus and M. E. Fine, J. Am. Cer. Soc. 55 (1972) 568.

17. W. C. Johnson and D. F. Stein, J. Am. Cer. Soc. 58 (1975) 485.

18. W. C. Johnson, Met. Trans. A, 8A (1977) 1413.

19. D. R. Clarke, J. Am. Cer. Soc. 63 (1980) 339.

20. W. C. Johnson (private communication, 1979).

21. A. G. Evans and A. Rana, Acta Met. 28 (1980) 129.

22. J. B. Wachtman and D. G. Lam, Jr., J. Am. Cer. Soc. 42 (1959) 254.

23. K. F. A. Walles, Proc. Brit. Cer. Soc. 15 (1970) 157.

24. D. E. Grady and J. Lipkin, Geophys. Res. Let. 7 (1980) 255.

25. D. E. Grady and M. E. Kipp, "Oil Shale Fracture and Fragmentation at High Rates of Loading," Sandia Report SAND-79-0563C (1979).

26. D. E. Grady and R. E. Hollenbach, "Rate-Controlling Processes in the Brittle Failure of Rock," Sandia Report SAND-76-0659 (1977).

27. D. E. Grady and M. E. Kipp, Int. J. Rock Mech. Min. Sci. & Geophys. Abstr. 16 (1979) 293.

28. W. Jannach, Int. J. Rock Mech. Min. Sci. & Geomech. Abstr. 14 (1977) 209.

29. J. Lankford, Geophys. Res. Let. (in preparation).

30. J. Lankford, J. Am. Cer. Soc. 62 (1979) 310.

II

THRESHOLD MICROFRACTURE DURING ELASTIC-PLASTIC INDENTATION OF CERAMICS

James Lankford

Department of Materials Sciences
Southwest Research Institute
San Antonio, Texas 78284, USA

ABSTRACT

It is shown that for a variety of ceramics, the threshold for microfracture during elastic-plastic indentation corresponds to radial, rather than subsurface median, crack formation. This is contrary to the fundamental assumption of current models for threshold crack nucleation by sharp indenters. The significance of this observation in terms of strength reduction is discussed.

1. Background

Models have recently been proposed [1,2] to predict the critical load and flaw size conditions which should prevail at the threshold for crack formation* (initiation) in ceramics subject to

---

*Crack formation is what can be measured in actual experiments. It consists of the critical flaw size, plus any crack extension which may have occurred during the indentation process; the latter is minimized in practice by carrying out tests as near the crack nucleation threshold as is possible.

elastic-plastic indentation. Both of the models explicitly deal with the initiation of subsurface median cracks,* the justification for which would seem to be twofold. First, median cracks have been demonstrated to exist, for example in soda-lime glass, as shown by Lawn and Evans [1]. Second, median cracks lend themselves to analysis, in that they are presumed to form beneath the indenter apex at subsurface origins, where indentation stress field analyses are relatively unperturbed by the constraint-free surface. Unfortunately, however, median cracks have not actually been shown to exist at the threshold.

In fact, there have been relatively few studies of indentation microfracture in which tests were performed at sufficiently low

---

*The Hagan model [2] is an effort to explain the seemingly too-large "fortuitous" flaws required by the Lawn-Evans model for alkali halides. This it does successfully, indicating that crack-nucleating flaws indeed can be deformation induced, rather than intrinsic. However, similar critical loads for median crack formation are derived. The idea of indenter deformation-nucleated flaws serving to initiate cracks should be applicable to radial cracks as well. Subsequent lateral crack formation is a separate issue not treated by either model.

loads to allow determination of the threshold load and crack size, and even less in which appropriate microscopic inspection was actually performed. Recently, the author carried out experiments to determine indentation threshold crack sizes and loads for a variety of crystalline ceramics, including fine-polished Al_2O_3, SiC, Si, as-grown Ge, and cleaved NaCl. Several factors related to the question of radial versus median threshold microfracture were established [3,4], as briefly summarized here. First, for all five materials, the lengths of the individual surface traces (C', Fig. 1) of the cracks formed by the threshold load, determined by SEM observation and acoustic emission, were in excellent agreement with threshold critical flaw sizes predicted by the Lawn and Evans model. Thus, if the surface traces had represented the intersection of median cracks with the surface, the "parent" median threshold cracks would have necessarily been extremely large, much larger than predicted by the model. Moreover, no acoustic emission was detected below the apparent threshold for radial cracking, so that should the threshold surface traces and the associated, initial acoustic emission have been caused by median cracking, the threshold median cracks for each material would have intersected the surface over a distance which just happened to agree with the predicted size of the threshold flaw, a highly improbable situation. It thus appears extremely likely that the observed surface traces represented radial crack formation.

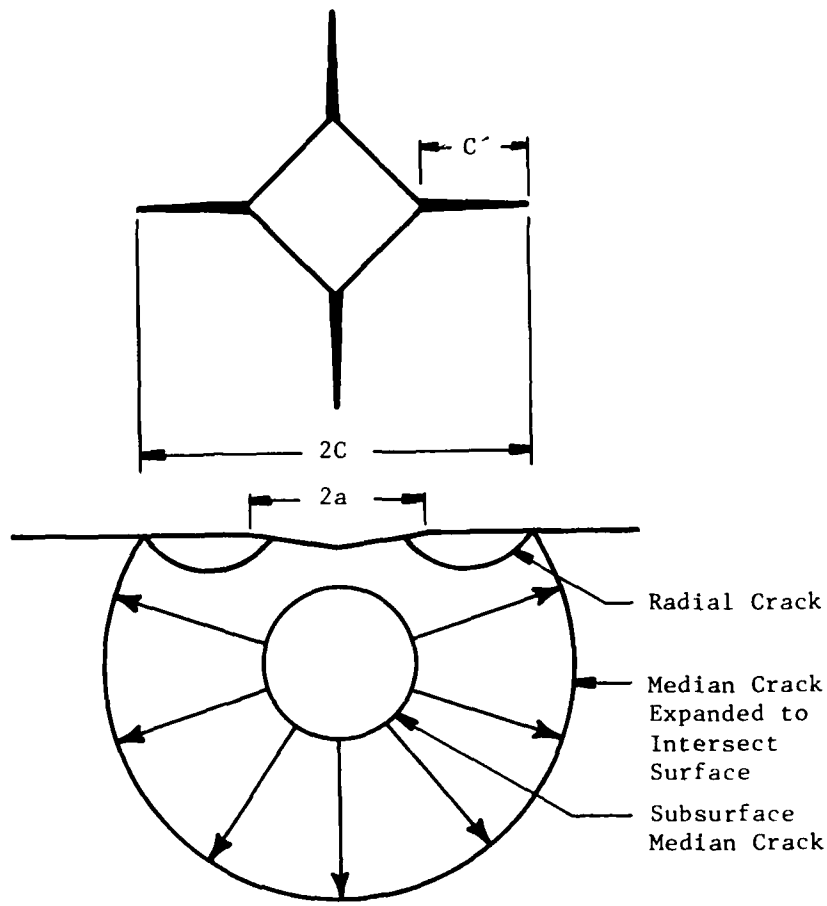

Figure 1. Radial versus median indentation microfracture patterns which produce a common surface trace C´.

These indirect inferences as to the prevalence of radial rather than median threshold cracking were supported by direct observation in two dissimilar ceramic systems. Radial cracking, to the absolute exclusion of median cracking, was observed optically [3] in transparent NaCl, and verified by acoustic emission, i.e., no acoustic emission was detected for loads below the radial crack threshold. In addition, specimens of SiC were cleaved through indentations formed by loads just above the ~10 gm threshold load for cracking [4]. SEM inspection showed (Fig. 2) that the subsurface indentation regime typically was devoid of median cracks, while prior to cleavage, radial cracks were present at the corners of each indentation.

2. New Experiments

In order to assess the generality of these inferences and observations suggesting radial rather than median threshold crack formation, experiments have now been extended to other materials. For example, loads P ranging from 50 to 500 gm were applied to polished (0.05 μm diamond) Lucalox* polycrystalline Al_2O_3. The microcracked indentations were then serial polished down from the original surface in ~1 μm increments, using large indentations as references. It was found that at relatively low loads (50-200 gm),

---

*G.E. Lamp Glass Division, Cleveland, Ohio.

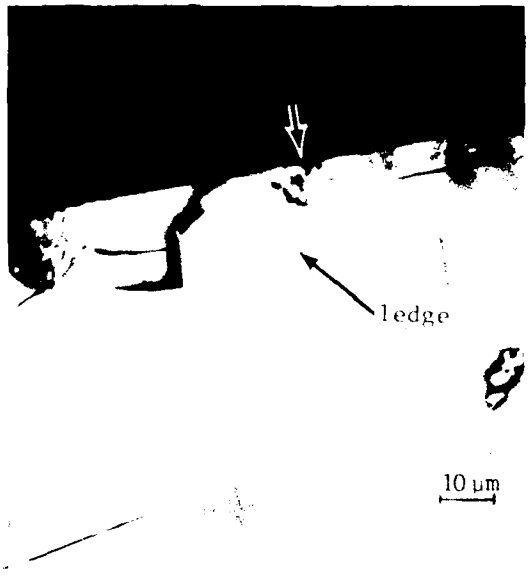

Figure 2. Subsurface damage attending indentation (arrow) produced in SiC by 200 gm load; ledge formed by intersecting radial crack segments. No median crack formation.

but above the microfracture threshold load of ~25 gm, only radial cracks were present (Fig. 3), with no discernible traces of median cracks beneath the indents (Although the indentations were gradually removed during polishing, their positions were indexed, for observational purposes, on the larger reference indentations which remained. Thus, the positions which the medians would have occupied were precisely fixed.). At higher loads (200 gm < P < 500 gm), the radial cracks apparently began to link up below the indentations, without necessarily cracking them, forming an annular configuration. Finally, for $P \gtrsim 500$ gm, the cracks began to crack across the indentations, assuming the form of half-penny surface cracks.

The observation of median cracks in glass apparently has been the principle basis for considering median crack formation to constitute the threshold. However, the median crack in soda-lime glass shown by Lawn and Evans (Fig. 1, Ref. 1) was 2 mm in diameter, produced by a load of 250 N; this certainly was not a threshold crack. Actually, recent observations reported by Hagan and Swain [5] indicated that for sufficiently low loads, i.e., $\lesssim$ 300 gm, radial cracking may occur in soda-lime glass without the occurrence of median cracking; therefore, the following experiment was performed. An annealed soda-lime glass slide was subjected to diamond pyramid indentation at various loads, from 10 to 2000 gm. Scanning electron microscopy was used to determine the threshold load for

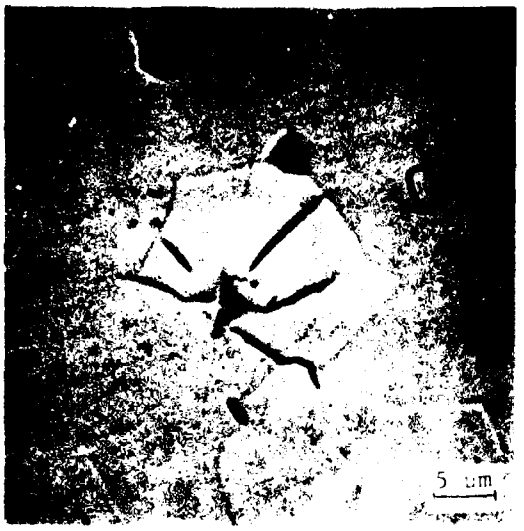

(a) Surface traces of microfracture pattern prior to sectioning.

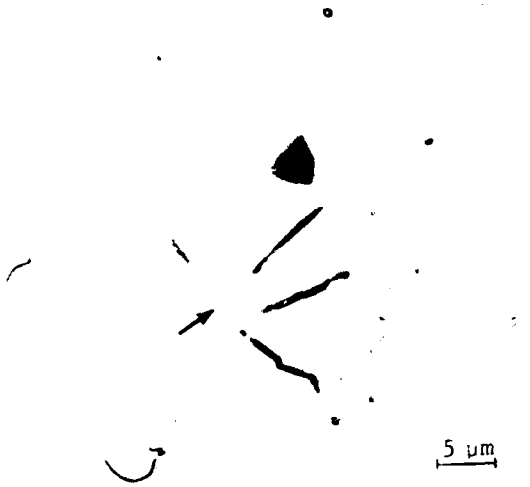

(b) Subsurface crack pattern after 1 μm of material removal. Indentation gone, radial cracks visible (arrow indicates locus of indent apex), no median cracks visible.

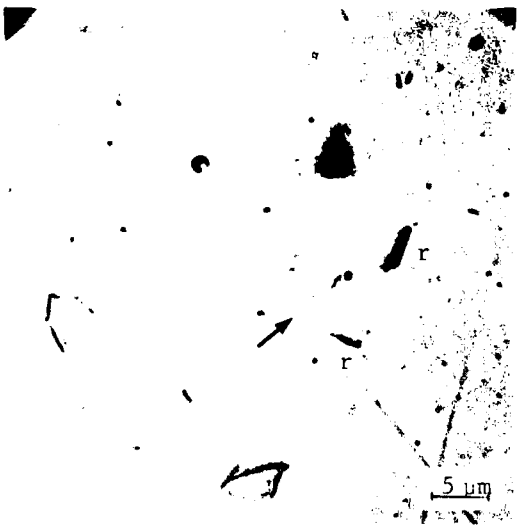

(c) Subsurface crack pattern after 3 μm of material removal. Radial cracks (r) barely visible (arrow indicates locus of indent apex), no median cracks visible.

Figure 3. Serial sectioning of 100 gm indent in Al_2O_3.

the appearance of indentation corner cracks. The indentations, which were lined up in a row, were then cleaved by a single crack passing through the array; indentation subsurface crack morphology was characterized using the SEM.

It was found that the threshold load for indentation corner crack nucleation was approximately 25 gm. Fig. 4 shows typical subsurface damage associated with indentations formed under these conditions. In many cases, lateral (L) as well as radial cracks form, but median cracks are always absent. This is particularly apparent in Fig. 4a; not only is no median crack visible, the outlines of the two radial cracks which formed in the plane of the cleavage section are clearly discernible. The bars above the cracks, which represent the average extent of the surfaces traces $2(C' + a)$ for $P = 300$ gms, correlate well with the tips of the radial crack outlines. At 2000 gms, the indentation corner cracks (Fig. 5) are what have been termed [6] "well-developed," i.e., extending well beyond the central deformation zone. However, even at this stage they clearly are not yet half-pennies, since they have no subsurface median component (Fig. 4b), but remain unconnected radial cracks attached to a central indentation. The ledge in Fig. 4b indicates where the two radials in the plane of cleavage linked up during cleavage.

Identical experiments were carried out for Si crystals. Again the results were the same; for loads ranging from the threshold

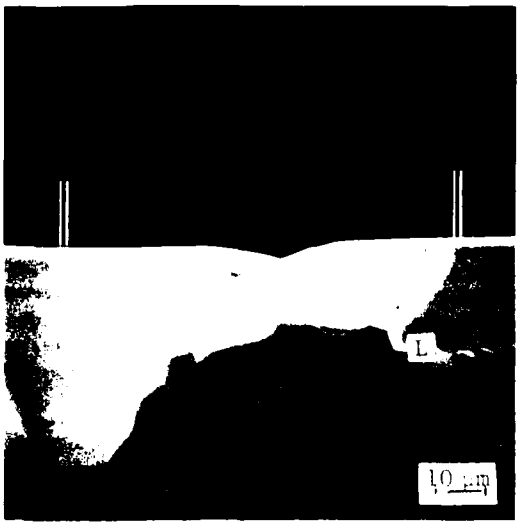

(b) P = 2000 gms. Lateral cracks (L) form, but no medians. Ledge produced by intersecting radial segments.

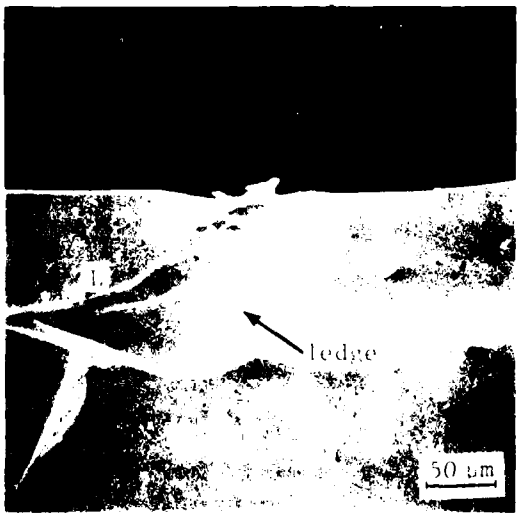

(a) P = 300 gms. Images of two radial cracks lying in the cleavage plane can be seen; tips correlate with average extent of 2(c' + a) for this load. Lateral cracking (L) occurs, but no median cracks have formed.

Figure 4. Subsurface damage attending indentation produced in soda-lime glass.

50 μm

Figure 5. Indentation corner cracks produced by 2000 gm load in soda-lime glass.

(~5 gms) up to 200 gms, no median cracks were present in sections cleaved through indents. Instead, the sections revealed subsurface ledges at which radial crack segments had linked up during cleavage.

For all five materials which have been discussed, as well as Ge, which seems to behave like Si, the relationship between $(C' + a)$ and P was established (Fig. 6) for loads including, and in excess of, the threshold, and found to be (approximately)

$$(C' + a) \propto P^{2/3} \tag{1}$$

with the proportionality constant depending upon material fracture toughness and indenter geometry [6]. This relationship is a crack growth law; it includes nucleation, but correlates the crack growth which takes place for loads in excess of the threshold. It is the same relationship which prevails at very high indentation loads, where the cracks formed are definitely half-penny shaped. Thus, there is a single functional representation which describes the growth of indentation corner cracks from an initial radial-plus-indentation configuration to a final half-penny geometry. There apparently is no subsurface median crack stage, but simply the joining of individual radial segments; this joining is clearly evidenced by the connective ledges which are often observed beneath the indentations (Figs. 2 and 4).

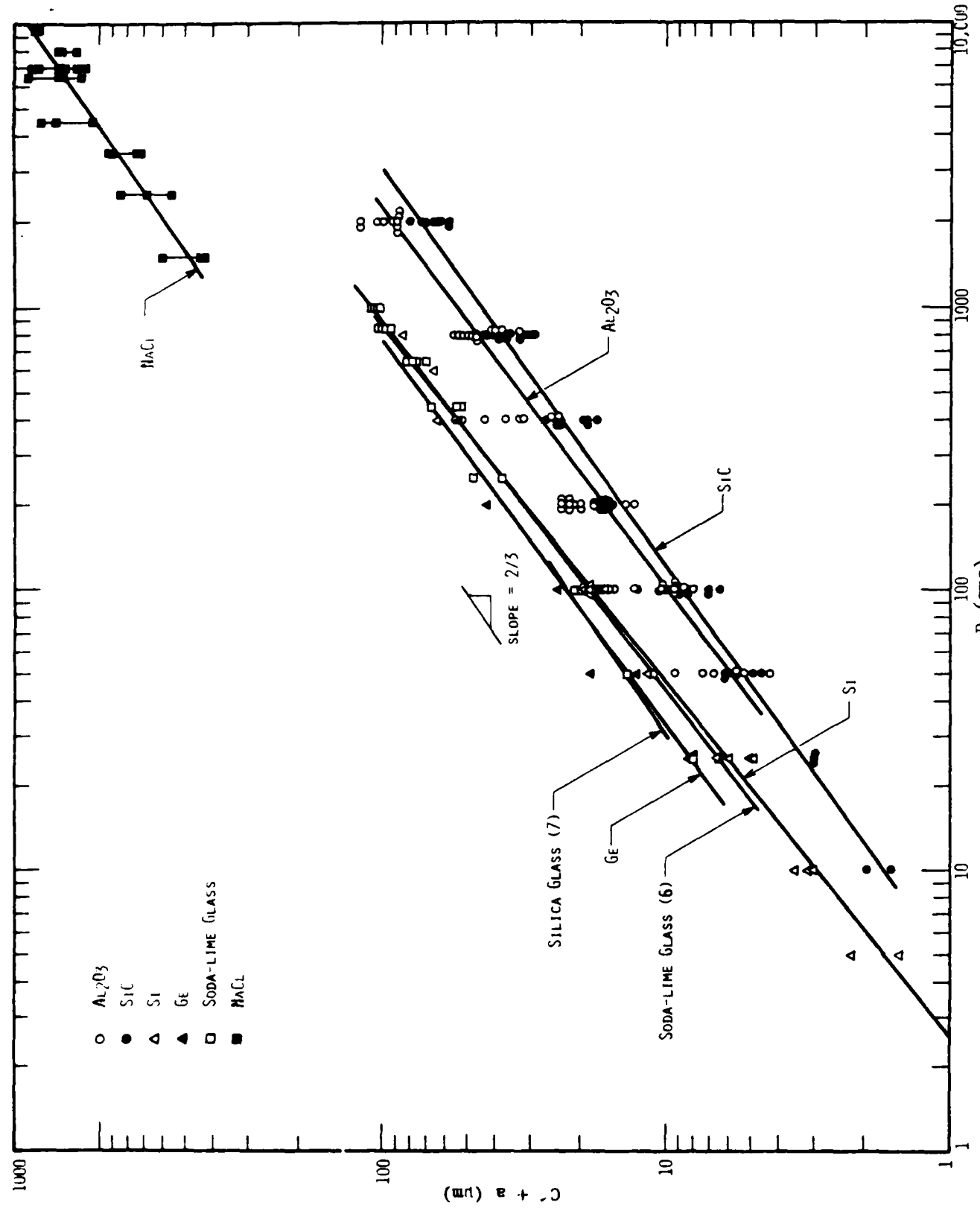

Figure 6. (C′ + a) versus P for various ceramics; data begin at the (approximate) threshold load in each case.

3. Discussion and Implications

The experiments described above provide reasonable evidence that radial cracks are the earliest strength-degrading cracks to form during the elastic-plastic indentation of many ceramics. The materials studied covered wide ranges in atomic bonding type, hardness, strength, toughness, and atomic order (crystalline versus amorphous). Acoustic emission did not occur for loads below the threshold loads required for indentation corner cracking. Sectioning, cleavage, and optical observation of transparent materials proved that the threshold surface traces were caused by radial cracks. The fact that no median cracks were observed for loads up to an order of magnitude higher than the radial crack threshold load indicates that median crack formation does not accompany the nucleation of radial cracks.

The data plotted in Fig. 6 provide indirect additional evidence in support of these conclusions. If the observed threshold surface traces represented the intersection of a large median crack with the surface, there should follow at higher loads a transient overshoot in $(C' + a)$ versus P, as the crack configuration changes to that of a half-penny by extending rapidly along the surface. This was not observed. Similarly, if the initial configuration (in a given plane) consisted of two radial cracks plus a subsurface median crack, a shift in $(C' + a)$ versus P should be observed,

corresponding to the load range in which the radial and median cracks grew together to form a half-penny. Again, this is not observed.

Since absolutely no shift or overshoot in the crack growth law was observed, the linear relationship between $(C' + a)$ and $P^{2/3}$ suggests that the radial-plus-indent flaw can be treated as a composite crack of total dimension $2(C' + a)$ in predicting above-threshold crack growth. Inspection of stress intensity solutions for holes with corner cracks, and for elliptical surface cracks of equivalent length [8], suggests by way of anology with the present problem, that for $C'/a \gtrsim 1$ (true for all loads in the present case), the stress intensity at the surface should not be significantly different for radial (length C') and half-penny (length $2C$) cracks at indentations where $(C' + a) = C$. This would support $C \propto P^{2/3}$ for both crack configurations, as observed. Moreover, recent experiments by Dabbs, et al [7] have shown that the strength degradation of glass specimens indented at loads just above the crack formation threshold* could be predicted using the fracture mechanics relationship for an assumed half-penny crack of length $2C$. This effectively treats the radial-plus-indent combination as a single flaw of total dimension $2(C' + a)$.

---

*The threshold in these experiments was based on observation of surface traces of corner cracks; considering the present work, this would correspond to radial cracking as in Fig. 4.

The indentation load required to produce a threshold crack is critically dependent upon the crack initiation process. The Lawn and Evans model, although attractive in general, errs in its quantitative prediction of the threshold load [3], principally because of its assumption that the threshold relates to median cracking. This assumption leads to calculation of threshold loads based on the application of Hill's solution for an internally pressurized, spherical cavity situated (conceptually) at the subsurface tip of the indenter. If the assumption is made instead that the threshold involves radial cracking, a different, more difficult stress analysis, dealing with tensile stresses near the indenter but at the surface, must be carried out. The author has applied the only current analysis which treats this problem, that of Perrott [9], to the model of Lawn and Evans, i.e., by simply substituting for the stress field. The loads predicted by this modified model are shown [3] to be much lower, in fact, falling into agreement with experiment [3]. A very recent theoretical stress analysis of the elastic-plastic indentation problem by Evans, et al [10], agrees with the present findings in predicting surface radial, rather than subsurface median, initial crack formation.

Finally, in terms of strength reduction, it is much easier to nucleate flaws in engineering ceramics than would be predicted on the basis of the current models which assume a median crack threshold. While there may be a threshold load to form median

cracks, it would seem to be of such high magnitude as to be rather uninteresting compared to the much lower load regime for radial crack nucleation. Fortunately, the present results indicate that even in their earliest stages, the strength reduction of the initial radial-plus-indent flaws can be treated analytically as if the composite flaws were tiny, half-penny cracks.

ACKNOWLEDGEMENT

The writer is grateful for the support of the Office of Naval Research, Contract No. N00014-75-C-0668, during the course of this work.

REFERENCES

1. B. R. Lawn and A. G. Evans, J. Mater. Sci. 12 (1977) 2195.
2. J. T. Hagan, J. Mater. Sci. 14 (1979) 2975.
3. J. Lankford and D. L. Davidson, J. Mater. Sci. 14 (1979) 1662.
4. J. Lankford and D. L. Davidson, J. Mater. Sci. 14 (1979) 1669.
5. J. T. Hagan and M. V. Swain, J. Phys. D 11 (1978) 2091.
6. B. R. Lawn, T. Jensen, and A. Arora, J. Mater. Sci. 11 (1976) 573.

7. T. P. Dabbs, D. B. Marshall, and B. R. Lawn, J. Am. Cer. Soc. 63 (1980) 224.

8. D. Broek, "Elementary Engineering Fracture Mechanics," Noordhoff, Leyden (1974).

9. C. M. Perrott, Wear 45 (1977) 293.

10. S. S. Chiang, D. B. Marshall, and A. G. Evans (in preparation).

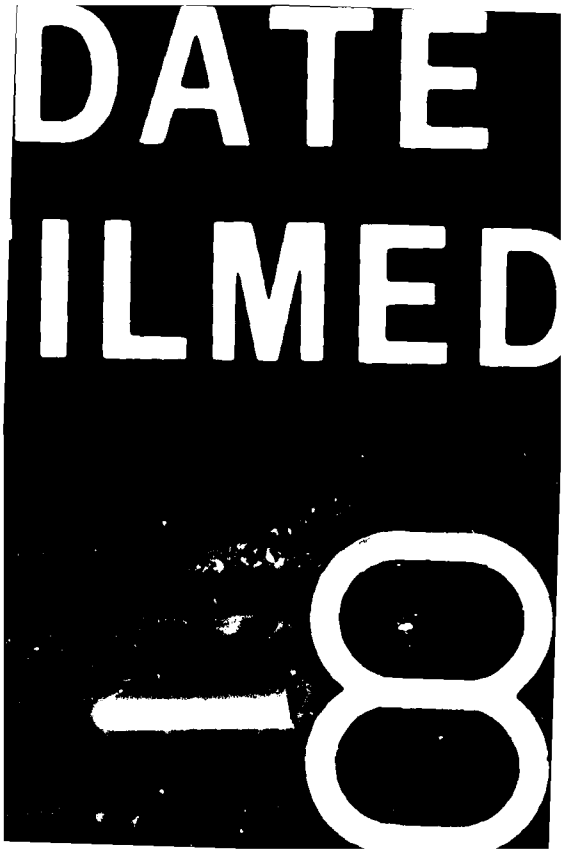
DATE
ILMED
8